Physica Scripta

PAPER

Magnetohydrodynamic nonlinear mixed convection flow of reactive tangent hyperbolic nano fluid passing a nonlinear stretchable surface

RECEIVED
6 August 2020

REVISED
18 October 2020

ACCEPTED FOR PUBLICATION
22 October 2020

PUBLISHED
9 November 2020

Ephesus Olusoji Fatunmbi[1], **Fazle Mabood**[2], **Hedi Elmonser**[3] **and Iskander Tlili**[4,5]

[1] Department of Mathematics and Statistics, Federal Polytechnic, Ilaro, Nigeria
[2] Department of Information Technology, Fanshawe College London, ON Canada
[3] Mathematics Department, College of Science, Al-Zulfi, Majmaah University, Al-Majmaah 11952, Saudi Arabia
[4] Institute of Research and Development, Duy Tan University, Da Nang 550000, Vietnam
[5] Faculty of Civil Engineering, Duy Tan University, Da Nang 550000, Vietnam

E-mail: iskandertlili@duytan.edu.vn

Keywords: mixed convection, tangent hyperbolic nano fluid, nonlinear radiation, activation energy, brownian motion

Abstract

The intent of this paper is to unravel the transport of a nonlinear mixed convection tangent hyperbolic nanofluid along a nonlinear stretchable sheet in the neighbourhood of a stagnation point. The impacts of magnetohydrodynamic, thermophoresis, Brownian motion and activation energy together with non-uniform heat source associated with varying thermal conductivity are scrutinized. The outlining transport equations are mutated into a system of nondimensional ordinary differential equations by the use of similarity transformations and then tackled with the Runge–Kutta Fehlberg coupling shooting method. The impact of all essential parameters in respect of the dimensionless quantities are graphically exhibited and deliberated. The significant consequences of the investigation are that increment in the Darcy with magnetic term declines the flow velocity while that uplift the fluid temperature. The skin friction factor triggers a considerable increase with the power-law exponent and magnetic field parameters. The intensity of heat and mass transfer shrink with hike in the values of the thermophoresis parameter. The vetting of the numerical solution is done with earlier related studies in the limiting position and presented in tabular form showing perfect correlation.

1. Introduction

There are various branches and mathematical formulations capturing the transport of the non-Newtonian fluids which have been proposed by researchers in the literature due to wide and varied physical properties of these fluids. Hence, it becomes impossible to comprehensively describe these fluid attributes in a single model. One of these models which characterizes the non-Newtonian fluid attributes by its shear-thinning nature is the tangent hyperbolic fluid. This model is simple and attractive and its preference over other constitutive non-Newtonian models stems from the fact that its constitutive laws are deduced from the theory of molecular kinetic as against conventional empirical relations. Common examples of fluids that characterize the tangent hyperbolic properties include the biological and industrial fluids (e.g. blood, ketchup, paints, melts solution and polymers). Due to its importance, various researchers have reported such fluids on different geometries. For example, Ullah *et al* [1] numerically reported the transport of such fluids prompted a stretchable sheet with internal heat source associated with Lie group analysis, Mahdy [2] discussed numerically tangent hyperbolic nanofluid flow configured in a stretchable cylinder with non-uniform temperature whereas Malik *et al* [3] analyzed such fluids using the same configuration coupled with magnetic field impact and reported that a higher flow resistance occurred with an enlargement of the material parameter and magnetic field term. Other relevant information on such investigations can be found in [4–6].

The term nanofluid is a description of fluids which consists of nanometer particles (made of metals, oxides, carbides, etc) suspended in base fluids (water, oil, polymer solution, etc). Nanofluids exhibit improved thermal conductivity alongside heat transfer in comparison to the conventional base fluids. They also possess unique attributes that make them potentially useful in various industrial and engineering processes in heat transfer, pharmaceutical processes, cooling of engines and vehicles, refrigerator, chiller and so on. Following the study of Choi and Eastman [7] and based on the immense applications, several reports have been given in literature on the transport of nanofluids coupled with Newtonian/non-Newtonian fluids and enclosed in different media. Abolbashari *et al* [8] generated results for the transport of Casson nanofluid activated by a stretched sheet coupled with convective wall situation and slip property. Of recent, Alsaedi *et al* [9] offered an analytical report on such subject with the use of Eyring-Powell nanofluid associated with Ohmic heating and thermophoresis effect. More reports on this concept can be obtained in [10–12].

Stagnation point flow describes a region of highest static pressure where at the same time the heat transfer and mass deposition attain maximum level whereas the velocity is zero. The applications of such a phenomenon can be encountered in the engineering and industrial operations including the cooling of electronic appliances by fans, thermal oil recovery, the extrusion of polymers in melt-spinning processes and so on. Pioneering such a study, Hiemenz [13] worked on a two-dimensional flat sheet. Afridi *et al* [14] conducted an analysis on such phenomenon engaging a Newtonian fluid enclosed in a stretchable sheet with Ohmic heating and entropy generation, Khalil-Ur-Rehman *et al* [15] discussed such subject with Eyring-Powell fluid and pointed out the existence of boundary layer formation only if the magnitude of the free stream velocity overrides the stretching velocity while Animasaun [16] as well as Fatunmbi and Adeniyan [17] engaged micropolar fluid to investigate such a topic on a steady stretchable sheet with an internal heat source. Other scholars have also investigated such a concept as found in [18–20].

Meanwhile, various industrial and engineering processes like fibrous insulation, ceramics production, combustion and biochemical systems, fog formation and so on are concerned with the phenomenon of chemical reaction coupling activation energy. Activation energy defines the least quantity of energy needed for the occurrence of a chemical reaction, in other words, it defines the smallest energy required to transform the species that change the reactants into products, its presence aids the rapid flow of particles. Ramzan *et al* [21] presented a model of reactive micropolar fluid flow with activation energy influenced by nonlinear thermal radiation while Alsaadi *et al* [22] applied an analytical approach through HAM to discuss the importance of activation energy for the flow of Williamson nanofluid. The authors highlighted that a rise in activation energy favours the concentration distribution. Khan *et al* [23] investigated numerically such a concept on a stagnation point flow with the impact of buoyancy forces whereas the flow of Carreau fluid coupled with activation energy with Cattaneo-Christov condition was reported by Kumar *et al* [24].

In many engineering processes and material manufacturing which require high temperature (e.g Nuclear power plants, hot rolling, heat exchangers, electrical power generation), the knowledge of thermal radiation is important for the construction of relevant devices. Generally, the radiative heat flux can be modelled as linear or nonlinear types depending on the magnitude of temperature difference that exists within the flow. The linear type is operative in the case of low temperature difference whereas the nonlinear type is relevant for the situations of low and high temperature differences. Of recent, Al-Khaled *et al* [25] conducted research showing the significance of such a concept in the transport of a reactive tangent hyperbolic fluid while Khan *et al* [26] using the same fluid to study the impact of nonlinear radiation associated with an internal heat source in the neighborhood of a stagnation region. For wider applications of thermal radiation, the present study has incorporated the general nonlinear thermal radiation model as investigated by [27–29].

The investigation of a mixed convection transport along a linear stretchable sheet coupled with magnetic field effect has been studied owing to its huge engineering as well industrial applications which includes: the cooling of nuclear reactor, metallurgical and extrusion activities, glass blowing, crystal growing, production of glass fiber, etc The previous researchers, however, took into account the case a linearly stretching sheet as initiated by Crane [30]. However, researches have shown that the stretching sheet velocity may depart from been linear in some practical situations. It can be exponential and/nonlinear as firstly reported by Gupta and Gupta [31] and extended by quite a several of scholars (see [32–37]). A mixed convection phenomenon occurs where natural and forced convection are combined. Such a situation is found applicable in drying processes, cooling of fans and electronic appliances, solar power collectors and so on. The previous studies have assumed a linear variation of density in the buoyancy force term. However, the existence of a large temperature difference between the surface and the ambient requires a nonlinear density with temperature and concentration. Hence, it becomes imperative to consider such concept as it affects the field of flow, heat, and mass transfer as studied by [26, 38–40].

The aim of the present study therefore is to carry out an investigation on the flow of nonlinear mixed convection in a reactive tangent hyperbolic nanofluid towards a stagnation point configured in a nonlinear stretchable sheet in a porous enclosure. The formulated model in this work incorporates the impacts of variable

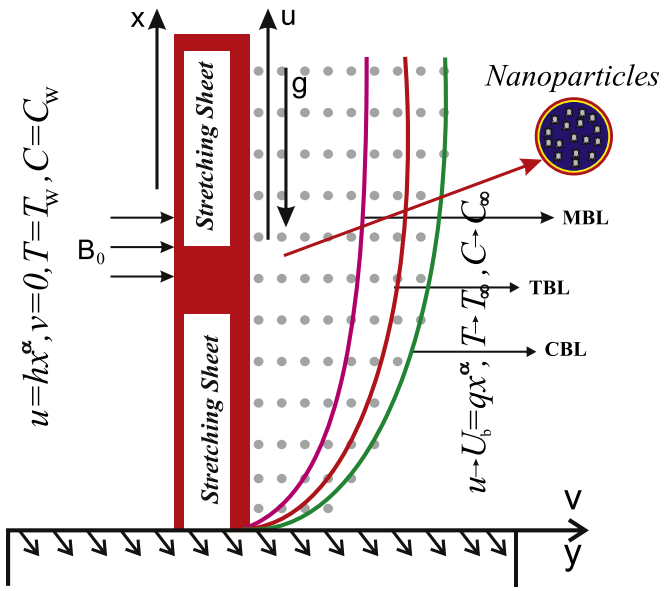

Figure 1. The Flow Configuration.

thermal conductivity along with non-uniform heat source, activation energy associated with prescribed surface temperature and concentration boundary conditions.

2. Problem development and governing equations

Taking into consideration an incompressible, steady transport of a tangent hyperbolic nanofluid passing a two-dimensional stretchable zero mass flux sheet in the neighborhood of a stagnation point. Taking the coordinate system of the flow to be $(x,\ y)$ with the respective velocity components indicated as $(u,\ v)$ with x axis being the flow direction while y axis runs perpendicular to it as depicted in figure 1. The nonlinear stretching sheet has the velocity $u = U_s = hx^{\alpha}$ (see figure 1) whereas the upstream velocity is $u = U_b = qx^{\alpha}$ where $h > 0$, q and α are the stretching parameter, a constant which measures stagnation point flow potency and the nonlinear stretching term related to the surface stretching speed in that order. The externally imposed magnetic field is presented as $B(x) = B_0 x^{(\alpha-1)/2}$ [35], which runs in the same direction as y axis with the intent that the induced magnetic field is negligible on the basis of sufficiently little magnetic Reynolds number. The fluid thermal conductivity is temperature-dependent as presented in equation (10) while the thermal and nanoparticles concentration condition at the wall are prescribed as indicated in equation (9). The heat transfer is being influenced by Joule heating, viscous dissipation, nonlinear thermal radiation, non-uniform heat source with thermophoresis and Brownian motion whereas while the nanoparticles concentration equation is developed with chemical reaction associated with activation energy. The tangent hyperbolic nanofluid density ρ varies nonlinearly with temperature and concentration as ([38, 40, 41]) expressed in equations (1)–(2).

$$\rho(T) = \rho(T_\infty) + \left(\frac{\partial \rho}{\partial T}\right)_\infty (T - T_\infty) + \left(\frac{\partial^2 \rho}{\partial T^2}\right)_\infty (T - T_\infty)^2 + \ldots \tag{1}$$

$$\rho(C) = \rho(C_\infty) + \left(\frac{\partial \rho}{\partial C}\right)_\infty (C - C_\infty) + \left(\frac{\partial^2 \rho}{\partial C^2}\right)_\infty (C - C_\infty)^2 + \ldots, \tag{2}$$

where the expansion of equations (1)–(2) to the second order respectively yields

$$\frac{\rho - \rho_\infty}{\rho} = -\beta_1 (T - T_\infty) - \beta_2 (T - T_\infty)^2, \tag{3}$$

$$\frac{\rho - \rho_\infty}{\rho} = -\beta_3(C - C_\infty) - \beta_4(C - C_\infty)^2. \tag{4}$$

In figure 1, *MBL*, *TBL* and *CBL* respectively indicates Momentum boundary layer, Thermal boundary layer and Concentration boundary layers. Incorporating the principles of the boundary layer approximations alongside with the aforementioned assumptions, the underlisted are the equations describing the transport of the hydromagnetic tangent hyperbolic nanofluid [26, 42, 43].

$$\frac{\partial u}{\partial x} + \frac{\partial v}{\partial y} = 0, \tag{5}$$

$$\begin{aligned}\left(u\frac{\partial u}{\partial x} + v\frac{\partial u}{\partial y}\right) = U_b\frac{dU_b}{dx} + \frac{\mu_f}{\rho_f}(1-\kappa)\frac{\partial^2 u}{\partial y^2} + \frac{\mu_f}{\rho_f}\sqrt{2}\kappa\Gamma\frac{\partial^2 u}{\partial y^2}\frac{\partial u}{\partial y} - \frac{\sigma_f B(x)^2}{\rho_f}(u - U_b)\\ - \frac{\mu_f}{\rho_f K_p}(u - U_b) + g[\beta_1(T - T_\infty) + \beta_2(T - T_\infty)^2\\ + [\beta_3(C - C_\infty) + \beta_4(C - C)^2\end{aligned} \tag{6}$$

$$\begin{aligned}(\rho c_p)_f\left(u\frac{\partial T}{\partial x} + v\frac{\partial T}{\partial y}\right) = \frac{\partial}{\partial y}\left(k_f\frac{\partial T}{\partial y}\right) + (\rho c_p)_p\left(\frac{\partial T}{\partial y}\right)\left[\frac{D_T}{T_\infty}\left(\frac{\partial T}{\partial y}\right) + D_B\left(\frac{\partial C}{\partial y}\right)\right]\\ + \sigma_f B(x)^2(u - U_b)^2 + \frac{\mu_f}{K_P}(u - U_b)^2\\ + \mu_f\left((1-\kappa)\left(\frac{\partial u}{\partial y}\right)^2 + \frac{\Gamma\kappa}{\sqrt{2}}\left(\frac{\partial u}{\partial y}\right)^3\right) + \frac{16\zeta^*}{3a^*}\frac{\partial}{\partial y}\left(T^3\frac{\partial T}{\partial y}\right) + q''',\end{aligned} \tag{7}$$

$$u\frac{\partial C}{\partial x} + v\frac{\partial C}{\partial y} = D_B\frac{\partial C^2}{\partial y^2} + \frac{D_T}{T_\infty}\left(\frac{\partial^2 T}{\partial y^2}\right) - k_1^2(C - C_\infty)\left(\frac{T}{T_\infty}\right)^r \exp\left(-\frac{E_1}{\lambda T}\right). \tag{8}$$

The accompanied boundary conditions for equations (5)–(8) are:

$$\begin{aligned}&u = U_s = hx^\alpha,\ v = 0,\ T = T_w(=T_\infty + Bx^{m_1}),\\ &C = C_w(=C_\infty + Dx^{m_2})\, when y = 0,\\ &u \to U_b = qx^\alpha,\ T \to T_\infty,\ C \to C_\infty,\ with\ y \to \infty.\end{aligned} \tag{9}$$

The expression for the thermal conductivity as relates to temperature is presented as [44],

$$k_f(T) = \frac{k_{f\infty}}{T_w - T_\infty}[(T_w - T_\infty) + \delta(T - T_\infty)]. \tag{10}$$

with k_∞ being the constant thermal conductivity while δ defines its parameter. In the energy equation (7), the last term (q''') indicates the non-uniform heat source which is model as

$$q''' = \frac{k_f U_s}{\nu_f x^\alpha}(Q_1 f' + Q_2\theta)(T_w - T_\infty). \tag{11}$$

The temperature/space dependent heat source is Q_2/Q_1, $\nu_f = \frac{\mu_f}{\rho_f}$ *is the kinematic* furthermore, the modified Arrhenius term is given in equation (8) as $K_1^2(C - C_\infty)\left(\frac{T}{T_\infty}\right)^r \exp\left(-\frac{E_1}{\lambda T}\right)$ with $K_1^2 = K_2^2 x^{\alpha-1}$ being the chemical rate. The permeability of the porous medium in equation (6) is indicated as $K_p = K_0 x^{1-\alpha}$, where K_0 is a constant [45, 46]. The underlisted dimensionless variables are introduced into the main equations.

$$\eta = \sqrt{\frac{h(\alpha+1)x^{\alpha-1}}{2\nu_f}}y,\ \psi = \sqrt{\frac{2\nu_f h x^{\alpha+1}}{\alpha+1}}f(\eta),$$
$$\theta(\eta) = \frac{T-T_\infty}{T_w-T_\infty},\ Nr = \frac{16\zeta^* T_\infty^3}{3a^* k_\infty},\ Re = \frac{U_s x}{\nu_f}$$
$$\phi(\eta) = \frac{C-C_\infty}{C_w-C_\infty},\ u = \frac{\partial\psi}{\partial y},\ v = -\frac{\partial\psi}{\partial x},$$
$$Nt = \frac{(\rho c_p)_p D_T(T_w-T_\infty)}{(\rho c_p)_f T_\infty \nu_f},\ H = \frac{q}{h},$$
$$Da = \frac{\nu_f}{hK_0},\ \theta_w = \frac{T_w}{T_\infty},\ \epsilon = \frac{(T_w-T_\infty)}{T_\infty},$$
$$Pr = \frac{\nu_f(\rho c_p)_f}{k_{f\infty}},\ M = \frac{\sigma B_0^2}{h\rho},$$
$$Gr_x = \frac{2g\beta_1(T_w-T_\infty)x^3}{(\alpha+1)\nu_f^2},\ Sc = \frac{\nu}{D_B},$$
$$Gc_x = \frac{2g\beta_3(C_w-C_\infty)x^3}{(\alpha+1)\nu_f^2},\ \lambda_1 = \frac{Gr_x}{Re_x^2},$$
$$N = \frac{Gc_x}{Gr_x},\ We = \Gamma\sqrt{\frac{h^3x^{3r-1}(\alpha+1)}{\nu_f}},$$
$$\zeta_2 = \frac{\beta_4(C_w-C_\infty)}{\lambda_1}Ec = \frac{U_w^2}{C_p(T_w-T_\infty)},$$
$$\gamma_1 = \frac{K_2^2}{h},\ E = \frac{E_1}{\lambda T_\infty},\ \zeta_1 = \frac{\beta_2(T_w-T_\infty)}{\lambda_1},$$
$$Nb = \frac{(\rho c_p)_p D_B(C_w-C_\infty)}{(\rho c_p)_f \nu_f}. \tag{12}$$

The substitution of quantities in (12) into the governing equations (5)–(8) yields:

$$((1-\kappa)+\kappa We f'')f''' + ff'' - \frac{2}{\alpha+1}(f'^2-\alpha H^2) - \frac{2(M+Da)}{\alpha+1}(f'-H) + \lambda_1\theta(1+\zeta_1\theta)$$
$$+\lambda_2\phi N(1+\zeta_2\phi) = 0, \tag{13}$$

$$\frac{1}{Pr}[1+\delta\theta+Nr(1+(\theta_w-1)\theta)^3]\theta'' + \frac{3Nr}{Pr}(\theta_w-1)\theta'^2(1+(\theta_w-1)\theta)^2$$
$$+\left(f\theta' - \frac{2m_1}{\alpha+1}f'\theta\right) + (N_t\theta'^2 + N_b\theta'\phi') + \frac{2Ec(M+Da)}{\alpha+1}(f'-H)^2$$
$$+Ecf''^2\left((1-\kappa)+\frac{We}{2}f''\right) + \frac{1}{Pr}\delta\theta'^2 + \frac{2(1+\delta\theta)}{\alpha+1}(Qf'+G\theta) = 0, \tag{14}$$

$$\phi'' + \frac{N_t}{N_b}\theta'' + Sc\left(f\phi' - \frac{2m_2}{\alpha+1}f'\phi\right) - Sc\gamma_1\left(\frac{2}{\alpha+1}\right)(1+\epsilon\theta)^r\exp\left(-\frac{E}{1+\epsilon\theta}\right)\phi = 0, \tag{15}$$

The boundary situations transform to:

$$f'(0) = 1,\ f(0) = 0,\ \theta(0) = 1,\ \phi(0) = 1.$$
$$f'(\infty) = H,\ \theta(\infty) = 0,\ \phi(\infty) = 0. \tag{16}$$

The table of nomenclature is presented in table 1.

The quantities of interest for the engineers are the coefficient of skin friction C_{fx}, the Nusselt number Nu_x and the Sherwood number Sh_x. These quantities are orderly presented as follows.

$$C_{fx} = \frac{2\tau_w}{\rho_f U_s^2},\ Nu_x = \frac{xq_w}{k_{f\infty}(T_w-T_\infty)},$$
$$Sh_x = \frac{xq_m}{D_B(C_w-C_\infty)}, \tag{17}$$

Table 1. Description of the Symbols.

Symbol	Description	Symbol	Description
a^*	Mean absorption coefficient	N	Ratio of concentration to buoyancy forces
C	Concentration	Nb	Brownian motion parameter
C_w	Concentration at the sheet	Nr	Ration parameter
C_∞	Concentration at the free stream	Nt	Thermophoretic parameter
Da	Darcy parameter	Pr	Prandtl number
D_B	Brownian diffusion coefficient	Q	Space-dependent heat source
D_T	Thermophoretic diffusion coefficient	r	Fitted rate constant $(-1 < r < 1)$
E	Activation energy	Sc	Schmidt number
Ec	Eckert number	T	Temperature
E_1	Coefficient of activation energy	T_w	Temperature at the sheet
g	Gravitational acceleration	T_∞	Temperature at free stream
G	Temperature-dependent heat source	u	Velocity in x direction
H	Velocity ratio parameter	U_s	Velocity at the sheet
K_1^2	Chemical reaction rate	v	Velocity in y direction
M	Magnetic field term	We	Weissenberg number
m_1/m_2	Temperature/concentration exponent	x, y	Cartesian coordinates
Greek	**Description**	**Greek**	**Description**
μ_f	Base fluid viscosity	ρ_f	Base fluid density
γ_1	Chemical reaction	ϵ	Temperature relative parameter
ν_f	Kinematic viscosity	κ	Power law exponent
β_1	Coefficient of linear thermal expansion	θ	Dimensionless temperature
β_2	Coefficient of nonlinear thermal expansion	θ_w	Temperature ratio term
β_3	Coefficient of linear concentration expansion	λ	Boltzmann constant (8.61×10^{-5} eV K^{-1})
β_4	Coefficient of nonlinear concentration expansion	λ_1	Mixed convection parameter
ζ_1	Nonlinear thermal convection term	λ_2	Mass mixed convection parameter
ζ_2	Nonlinear concentration convection	Γ	Relaxation time
ζ^*	Stefan-Boltzmann constant	$(\rho c_p)_f$	Effective heat capacity of fluid
σ	Electrical conductivity	$(\rho c_p)_p$	Effective heat capacity of nanoparticles

with

$$\tau_w = \mu_f\left[\frac{\partial u}{\partial y} + \frac{\Gamma}{\sqrt{2}}\left(\frac{\partial u}{\partial y}\right)^2\right]_{y=0},$$
$$q_w = -\left[\left(k_{f\infty} + \frac{16T^3\sigma^*}{3k^*}\right)\frac{\partial T}{\partial y}\right]_{y=0},$$
$$q_m = -\left(D_B\frac{\partial C}{\partial y}\right)_{y=0}, \tag{18}$$

where τ_w indicates surface shear stress, q_w represents surface heat flux and q_m denotes the surface mass flux in that order. Using equations (12) and (18), the dimensionless C_{fx} is written in equation (19) while that of Nu_x and Sh_x are respectively presented in equation (20).

$$Re_x^{\frac{1}{2}}C_{fx} = 2(\alpha+1)^{\frac{1}{2}}\left[(1+\kappa)f''(0) + \frac{We}{2}f''^2(0)\right], \tag{19}$$

$$Re_x^{-\frac{1}{2}}Nu_x = -\left(\frac{\alpha+1}{2}\right)^{\frac{1}{2}}[1 + Nr(1+(\theta_w-1)\theta(0))^3]\theta'(0),$$
$$Re_x^{-\frac{1}{2}}Sh_x = -\left(\frac{\alpha+1}{2}\right)^{\frac{1}{2}}\phi'(0). \tag{20}$$

3. Numerical method with validation

The system (13) to (15) subject to (16) depicts a boundary value problem with high degree of nonlinearity, thus, an exact solution to the system seems difficult to asses. In this view, an approximate numerical solution is sought

Table 2. Values of $f''(0)$ in comparison with [49, 50] as M changes when $\kappa = We = H = Da = \lambda_1 = \lambda_2 = N = 0$, $Pr = \alpha = 1.0$.

M	[49]	[50]	Present Study
0	1.000 008	—	1.000 00
	−1.414 2135	−1.414 21	−1.414 21
	−2.449 4987	−2.4494	−2.449 49
	−3.316 6247	−3.3166	−3.316 62
	−7.141 4284	−7.1414	−7.141 43
	−10.049 875	−10.0498	−10.049 89
	−22.383 029	−22.3830	−22.383 02
	−31.638 584	—	−31.638 63

Table 3. Values of $(-\theta'(0))$ as compared with [51] and [52] for variations in Pr when $m_1 = m_2 = \alpha = 1.0$ and $\delta = Nr = Ec = Q = G = M = H = Da = 0$.

Pr	[51]	[52]	Present Study
0.72	0.8058	0.8088	0.808 637
.0	0.9691	1.0000	1.000 000
.0	1.9144	1.9237	1.923 683
.0	3.7006	3.7207	3.720 674

by a famous shooting technique coupled with Runge–Kutta-Fehlberg method. Based on the popularity of this method as described and applied by many authors ([47–50]), we do not give its details here. We set $\kappa = We = \zeta_1 = \zeta_2 = N_t = N_b = m_1 = m_2 = 0.1$, $\theta_w = 1.3$, $Q = 0.01$, $Da = M = \delta = Nr = \lambda_1 = \lambda_2 = G = r = N = 0.2$, $Sc = \alpha = 1.0$ and $Pr = 2.0$ as parametric values unless listed otherwise in the plots. To crosscheck the credibility of the results obtained in the current study, a comparative analysis of $f''(0)$ for variations in M with previously reported data of Mabood and Das [49] and Xu & Lee [50] is reported in table 2 and a comparative study of $(-\theta(0))$ for different Pr with previously published results of Ali [51] alongside with Mabood and Shateyi [52] is recorded in table 3 which validate our code. The comparisons of solutions are shown in tables 2 and 3, reasonable agreement is obtained with earlier computations which confirm the validity of the present numerical solutions.

4. Presentation of results

The physical impacts of the selected parameters on the various dimensionless quantities are presented graphically (figures 2–11) and discussed in this section. The plots capturing the reactions of the velocity field versus η are presented in figures 2(a), (b) and 3(a)–(c) as various parameters vary. In clear terms, there is a decelerated flow as the magnetic field (M) parameter enlarges both in the existence or otherwise of the Darcy term (Da). Such a trend is induced by the action of the Lorentz force occasioned by the interaction of the transversely applied magnetic field and the electrically conducting tangent hyperbolic fluid.

Hence, a hike in M improves the Lorentz force and consequently compel a reduction in the flow regime. However, the velocity further reduced in the existence of the Darcy term ($Da = 1.0$) than in its absence ($Da = 0$). The power law exponent (κ) in the presence of the nonlinear stretching term (α) has a diminishing influence on the velocity regime as depicted in figure 2(b). This pattern resulted from an enhanced strength of viscosity as the magnitude of κ enlarges. Figure 3(a) informs that the increasing trend in the velocity ratio term (H) raises the velocity with or without the thermal conductivity parameter (δ). This estimation shows that a rise in H implies a higher upstream velocity leading to an accelerated fluid flow. An increasing trend of the mixed convection term (λ_1) boosts the velocity field (figure 3(b)) due a decline in the viscous force as λ_1 enhances. Likewise, higher values of the nonlinear thermal mixed convection term (ζ_1) induces a higher velocity as displayed in figure 3(b). This pattern occurs due to an improvement in $(T_w - T_\infty)$ as ζ_1 increases and at such, the velocity field is enhanced. The concentration nonlinear mixed convection parameter (ζ_2) and the ratio of concentration to thermal buoyancy forces parameter (N) propel accelerated velocity as showcased in figure 3(c).

Figure 4(a) reveals that a stronger magnetic field term (M) with or without the Darcy term raises the tangent hyperbolic fluid temperature. As noted earlier, a hike in M creates a drag in the fluid flow due to Lorentz force and as result an extra heat is being produced thus, the temperature uplifts. In a related sense, an increment in the power law exponent (κ) thickens the structure of thermal boundary layer such that the temperature is raised as

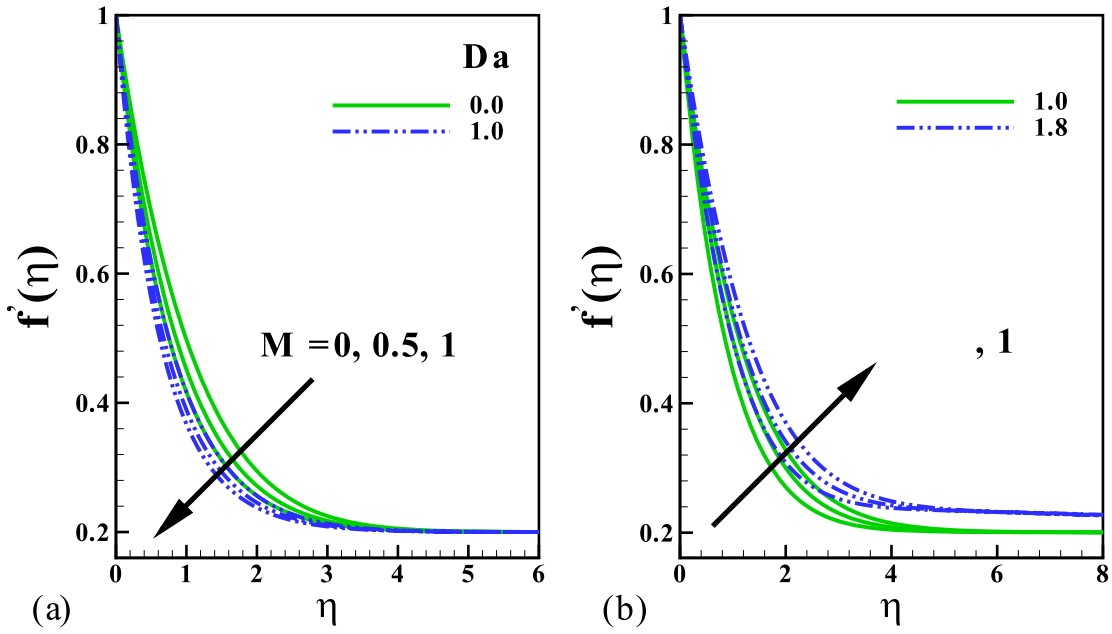

Figure 2. Plots of velocity distribution with variations in (a) M & Da (b) κ & α.

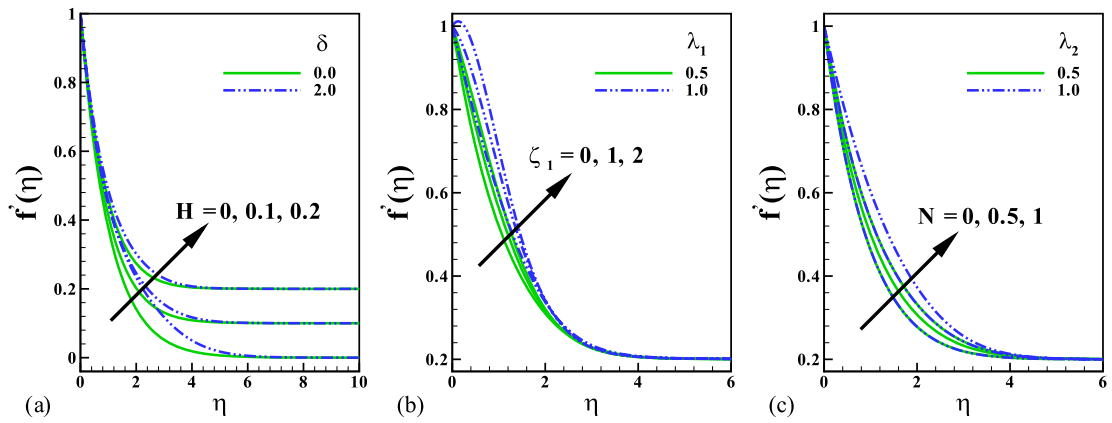

Figure 3. Curves of velocity for variations in (a) H & δ (b) ζ_1 & λ_1 (c) N & λ_2.

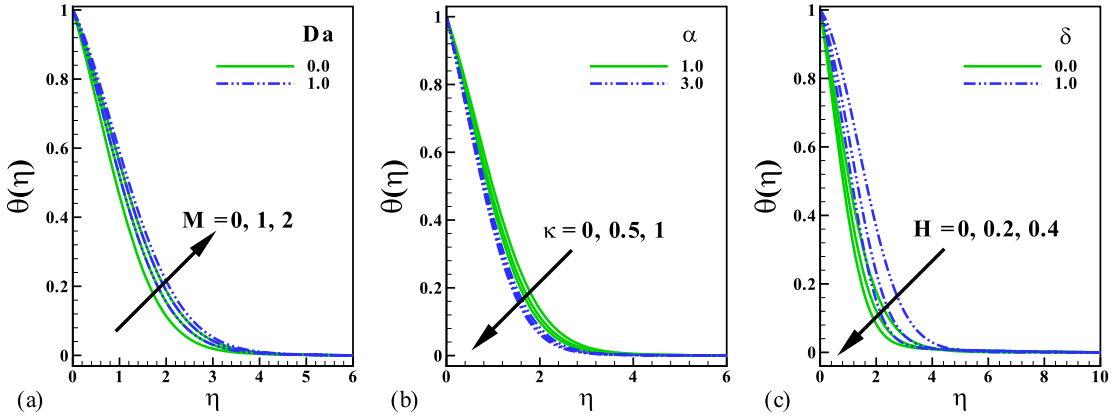

Figure 4. Graphs showing temperature profiles with variations in (a) M&Da (b) κ&α (c) H&δ.

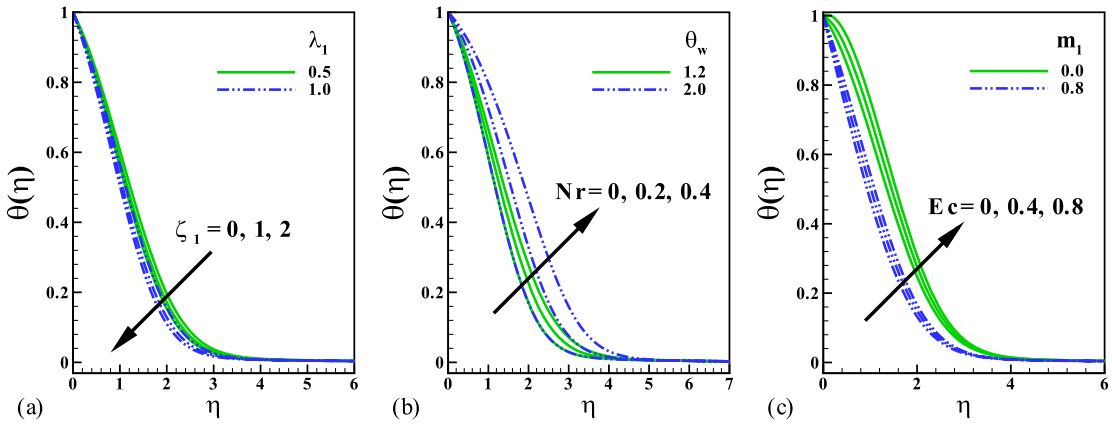

Figure 5. Curves of temperature field with changes in (a) ζ_1 &λ_1 (b) *Nr*&θ_w (c) *Ec*&m_1.

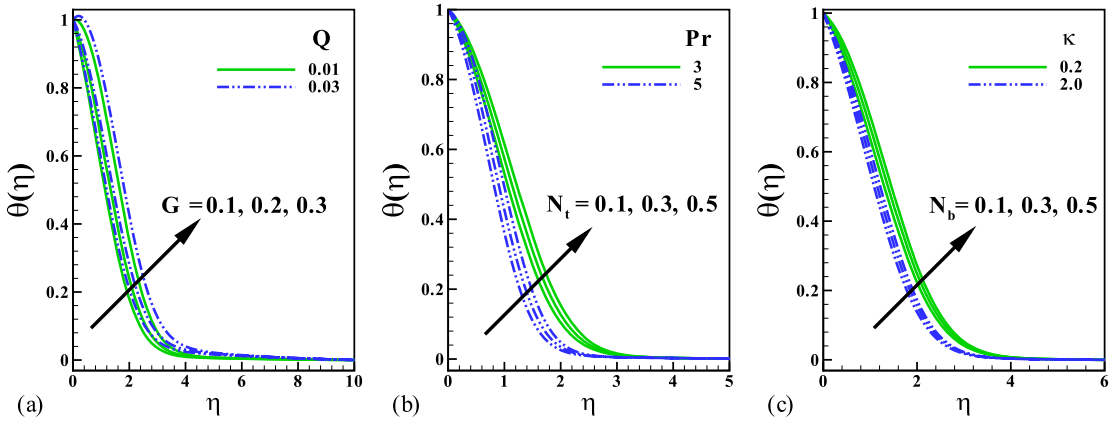

Figure 6. Plots showing temperature profiles with variations in (a) *G*&*Q* (b) N_t &*Pr* (c) N_b &κ.

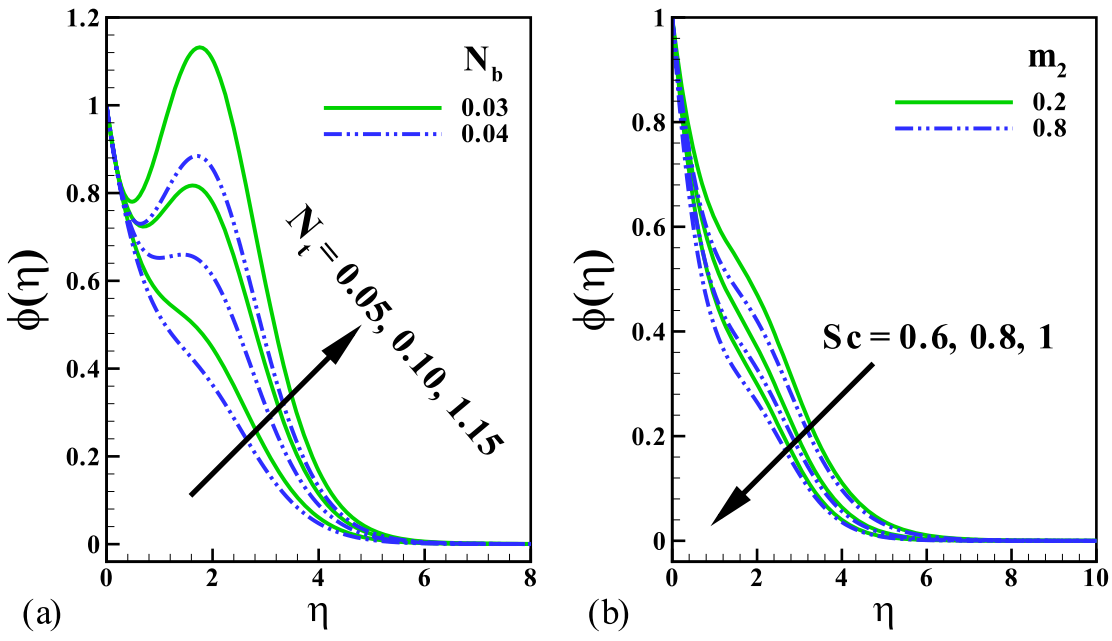

Figure 7. Plot of concentration field for variations in (a) N_t &N_b (b) *Sc*&m_2.

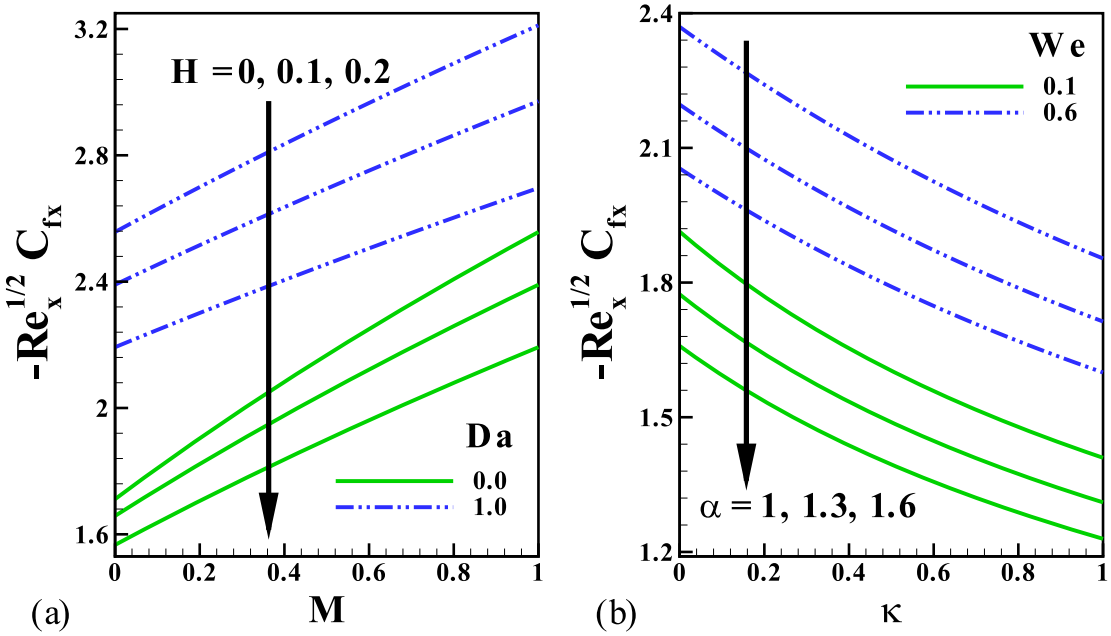

Figure 8. Graphs of concentration profiles for diverse values of (a) γ_1&r (b) E&ϵ.

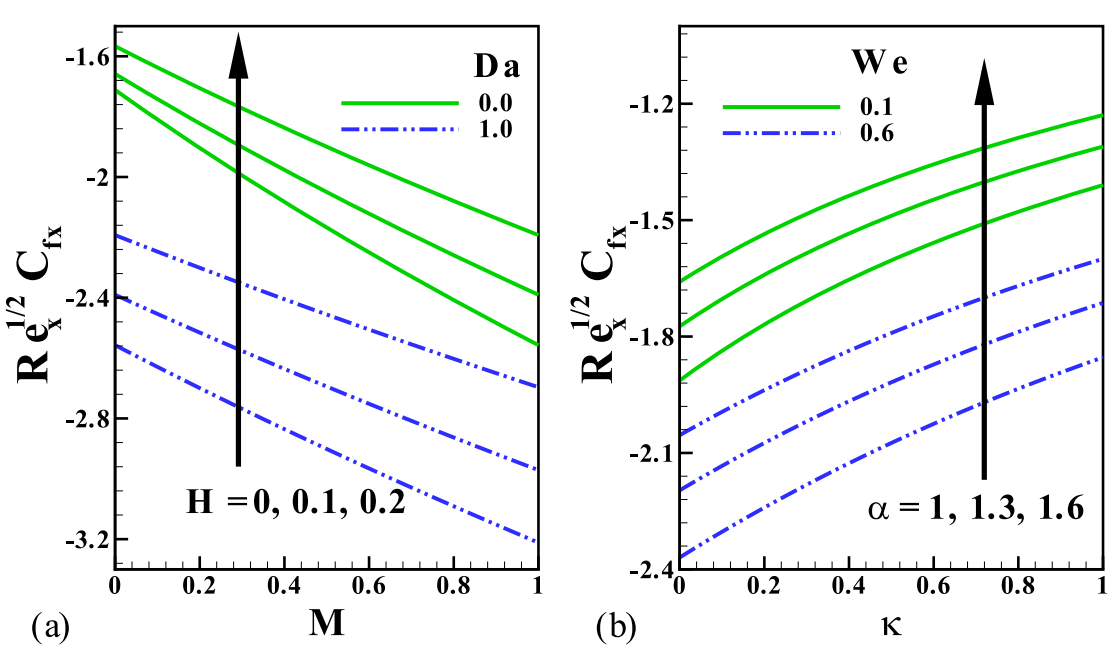

Figure 9. Plots of skin friction coefficient C_{fx} for variations in (a) H, Da&M (b) α, We&M.

described in figure 4(b). Contrarily, a downward pattern is noticed in the temperature when the strength of the velocity ratio term (H) advances whereas the converse is the case for growth in the thermal conductivity parameter (δ) as presented in figure 4(c).

The temperature field also declines with advancing trend of λ_1 and ζ_1 as illustrated in figure 5(a). On the other hand, the impact of the radiation term (Nr) is to enhance the temperature profiles as observed in figure 5(b). In the same vein, a rise in the temperature ratio parameter (θ_w) strengthens the thermal boundary structure and as well boosts the temperature profiles (figure 5(b)). From figure 5(c), it is discovered that there is an improvement in the tangent hyperbolic fluid temperature field due to a rising pattern of the Eckert number (Ec) resulting from the friction between the fluid particles. However, a thinner thermal boundary structure is exhibited with increasing trend of the temperature exponent term (m_1) which in turn facilitates a decline in temperature distribution.

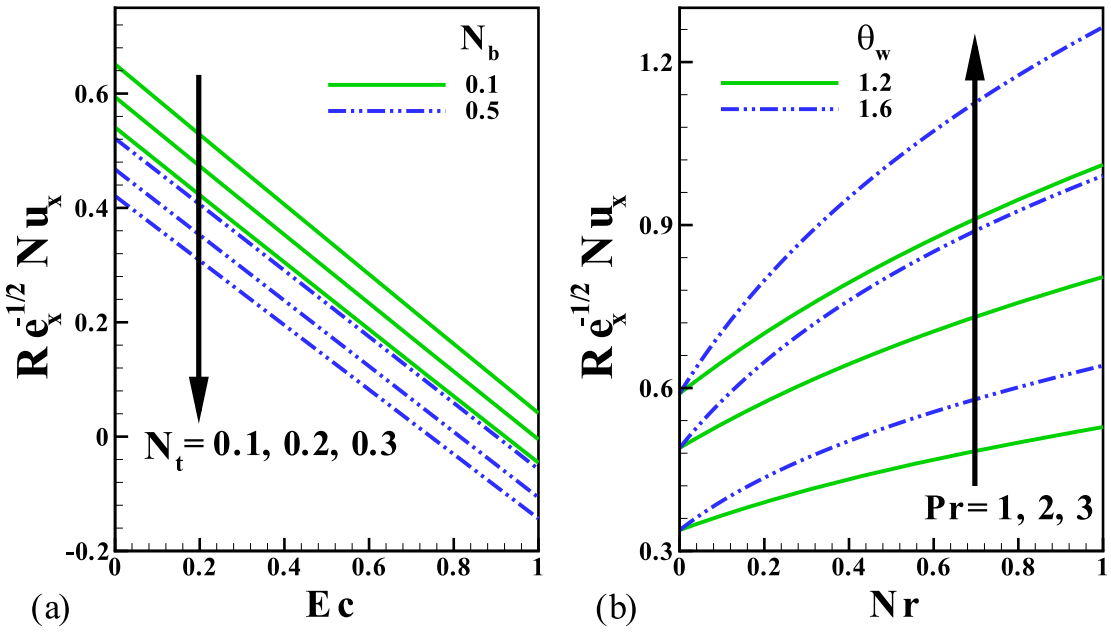

Figure 10. Graphs of Nusselt number for diverse values of (a) N_t, N_b& Ec (b) Pr, Nr & θ_w.

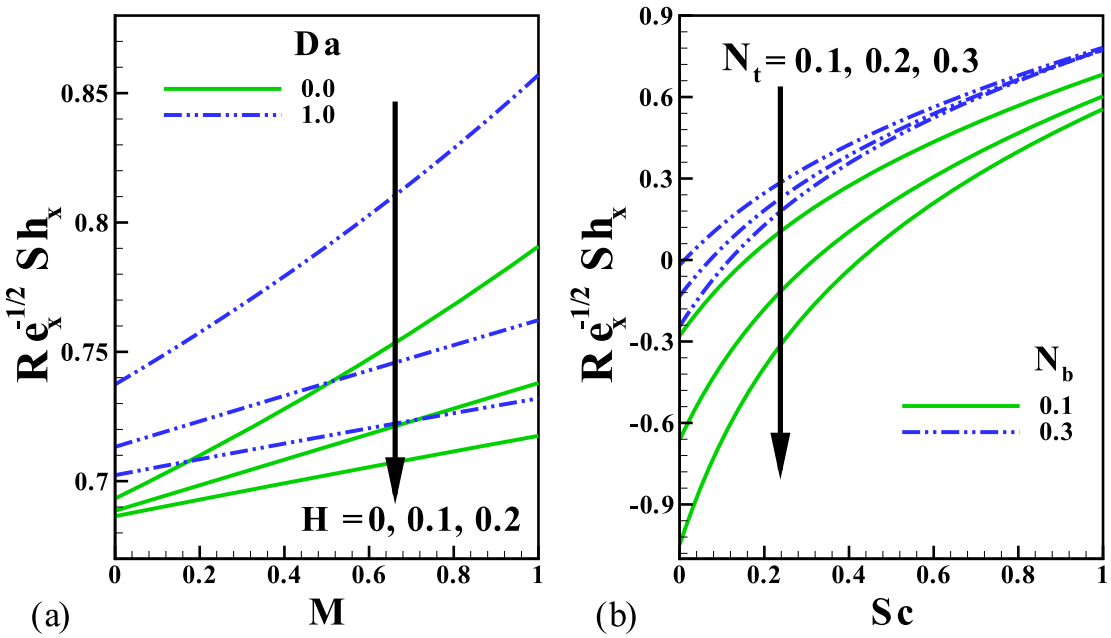

Figure 11. Curves of Sherwood number for changes in (a) H, Da&M, (b) N_t, N_b & Sc.

Figures 6(a)–(c) also depict the trend of the temperature field for variations in some selected parameters. From figure 6(a), the reaction of the temperature profiles to growth in the strength of both temperature-dependent heat source (G) and space-dependent heat source (Q) is plotted. Clearly, both terms create additional heat in the flow regime and thus enhance thermal field. Similarly, increasing the thermophoresis term (N_t) empowers the temperature profiles due to temperature gradient created by the thermophoretic force as displayed in figure 6(b) whereas an opposite trend occurs with a hike in Pr.

The temperature profiles also enlarge with a raise in the magnitude of the Brownian motion (N_b) as described in From figure 6(c). The Brownian motion corresponds to an irregular movement exhibited by the nanoparticles suspended in a base fluid. In respect to this irregular motion, there is a higher kinetic energy owing to the enhanced movement of the molecules of both the nanoparticles as well well as the base fluid which leads to an improved surface temperature.

Figures 7(a), (b) reflect the impact of some chosen parameters on the concentration field. It is evident that the concentration profile is strengthened in respect of growth in the thermophoresis term (N_t) whereas higher values of the Brownian motion parameter (N_b) decreases it. The rising pattern of the term defining the Schmidt number (Sc) and that of the concentration exponent term (m_2) propels a decline in the concentration boundary structure and consequently discourage the growth of the concentration field as demonstrated in figure 7(c). From figure 8(a), it is pointed out that the concentration field depletes with increasing trend of the chemical reaction term (γ_1). Here, higher γ_1 corresponds to higher rate of degenerative chemical reaction through which the species is dissolved more effectively and in consequence, there is a decay in the nanoparticles concentration field. The curves of the concentration profile to variations in the activation energy term (E) in the presence or absence of the temperature relative term (ϵ) is sketched in figure 8(b). A rise in E promotes a corresponding increase in the concentration profile. This trend reveals that an increase in E leads to a decline in the modified Arrhenius function which in turn propels a rise in the productive chemical reaction and at such, the concentration field becomes enlarged.

The structures of the skin friction coefficient as regards to some parameters are plotted in the figures 9(a), (b). It is obvious that an improvement in the velocity ratio term (H) tends to lower the skin friction coefficient but a boost in the magnetic field and Darcy terms energizes it as revealed in figure 9(a). An increment in the strength of Weissenberg number (We) with the power law exponent accelerates the coefficient of skin friction as demonstrated in figure 9(b) whereas the trend is reversed with rising values of α. In a related sense, the Nusselt number depletes with upward lifting of the thermophoresis (N_t), Brownian motion (N_b) and Eckert number parameters as showcased in figure 10(a). Contrarily, the uplifting of Prandtl number (Pr) with temperature ratio term (θ_w) creates an improvement in the heat transfer in the presence of thermal radiation as plotted in figure 10(b).

The mass transfer also improves with an uplift in the magnetic field (M), Darcy term (Da), Schmidt number (Sc) and Brownian motion (N_b) parameters as illustrated in figures 11(a), (b) whereas an opposite reaction exists with growing values of the velocity ratio (H) and thermophoresis (N_t) terms.

5. Conclusion

A physical model is developed for the thermo-solutal transport of a reactive tangent hyperbolic nanofluid in the neighbourhood of a stagnation point from a nonlinear stretchable sheet enclosed in a porous device. Also included in the model are the impacts of nonlinear thermal radiation and activation energy with MHD. The transformed dimensionless nonlinear boundary value problem has been solved with the Runge–Kutta Fehlberg coupling shooting technique. Validation with previous studies reveals perfect correlation in the limiting cases. A parametric study of the impact of selected variables on the transport characteristics has been constructed graphically. The simulations have shown that:

- Increment in the Darcy Da, power law exponent κ and magnetic field M terms lead to the diminution of the flow field while that of mixed convection λ_1 and nonlinear mixed (both thermal and concentration) convection uplifts it.
- Rise in the velocity ratio term H upsurges fluid velocity while that peters out the temperature.
- There is an improvement in the tangent hyperbolic fluid temperature with the increased values of the radiation Nr, heat source Q, thermophoresis N_t and Eckert number Ec parameters.
- Concentration is raised with the increased values of thermophoresis term N_t and activation energy term E but the reverse is the case for the Brownian motion N_b and chemical reaction term γ_1.
- Skin friction coefficient is strengthened due to higher magnetic M, power law exponent κ and Darcy parameters Da while a reversed trend occurred with a rise in H.
- Nusselt number appreciates in respect of the Prandtl number Pr, temperature ratio term θ_w and Nr while the opposite is the case for N_t, N_b and Ec.
- The mass transfer enlarges for incremental values of Da, M and Schmidt number Sc whereas it falls with thermophoresis term N_t.

Acknowledgments

Dr Hedi Elmonser would like to thank Deanship of Scientific Research at Majmaah University for supporting this work under the Project Number No. R-1441-182.

Data availability

The data that supports the findings of this study are available within the article.

References

[1] Ullah Z and Zaman G 2017 *Heliyon* **3** 1–15
[2] Mahdy A 2018 *Proc. Mech. Eng.* **0** 1–11
[3] Malik M Y, Salahuddin T, Hussain A and Bilal S 2015 *J. Magn. Magn. Mater* **395** 271–6
[4] Akbar N S, Nadeem S, Haq R U and Khan Z H 2013 *Indian J Phys* **87** 1–4
[5] Ullah Z, Zaman G and Ishak A 2020 *Chinese J. Phys.* **66** 258–68
[6] Salahuddin T, Malik M Y, Hussain A, Bilal S and Awais M 2015 *AIP Advances* **5** 1–13
[7] Choi S U S and Eastman J A *Enhancing Thermal Conductivity of Fluids with Nanoparticles (No. ANL/MSD/CP-84938; CONF-951135-29)* (Argonne National Lab.) *(IL United States)*
[8] Abolbashari H M, Fredoonimehr N, Nazari F and Rashidi M M 2015 *Adv. Powd. Tech.* **2015** 1–12
[9] Alsaedi A, Hayat T, Qayyum S and Yaqoob R 2020 *Comp. Meth. Prog. Biomed* **186** 1–9
[10] Hafeez A, Khan M, Ahmed A and Ahmed J 2020 *Appl. Math. Mech. -Engl. Ed.* **41** 1083–94
[11] Akbar N S, Nadeem S, Haq R U and Khan I 2013 *Chinese J. Aeronautic* **26** 1389–97
[12] Noor N F M, Haq R E, Nadeem S and Hashim I 2015 *Meccanica* **2015** 1–16
[13] Hiemenz K 1911 *Dingerls Polytech. J* **326** 321–4
[14] Afridi M I, Qasim M, Khan I and Tlili I 2018 *Case Stud Therm Eng* **12** 292–300
[15] Rehman K U, Malik M Y and Makinde O D 2018 *J King Saud Univ. Sci.* **30** 440–9
[16] Animasaun I L 2017 *J. Egypt. Math. Soc.* **25** 79–85
[17] Fatunmbi E O and Adeniyan A 2018 *J Adv. Math Comput Sci.* **26** 1–19
[18] Bhatti M M and Rashidi M M 2016 *Int. J. Appl. Comput. Math* **3** 1–15
[19] Mondal H and Bharti S 2020 *J. Appl. Comput. Mech.* **6** 1–12
[20] Agbaje T M, Mondal S, Makukula C G, Motsa S S and Sibanda P 2017 *Ain Shams Eng. J* **9** 233–43
[21] Ramzan M, Ullah N, Chung J D, Lu D and Farooq U 2017 *Sci. Rep.* **7** 1–15
[22] Alsaadi F E, Hayat T, Khan M I and Alsaadi F E 2020 *Comput Methods Programs Biomed* **183** 1–8
[23] Khan M I, Hayat T, Khan M I and Alsaedi A 2018 *Int. Commun. Heat Mass Transf.* **91** 216–24
[24] Kumar R V M S S K, Kumar G V, Raju C S K, Shehzad S A and Varma S V K 2018 *J. Phys. Commun.* **2** 1–15
[25] Al-Khaled K, Khan S U and Khan I 2020 *Heliyon* **6** 1–7
[26] Khan M I, Khan T A, Qayyum S, Hayat T, Khan M I and Alsaedi 2018 *Eur. Phys. J. Plus* **133** 1–20
[27] Mabood F, Imtiaz M, Alsaedi A and Hayat T 2016 *IJNSNS* **17** 221–9
[28] Gbadeyan J A, Titiloye E O and Adeosun A T 2020 *Heliyon* **6** 1–10.
[29] Fatunmbi E O and Adeniyan A 2020 *RINENG* **6** 1–10
[30] Crane L J 1970 *J. Appl. Math. Phy.* **21** 645–7
[31] Gupta P S and Gupta A S 1977 *Can. J. Chem. Eng.* **55** 744–6
[32] Cortell R 2007 *Appl. Math. Comput.* **184** 864–73
[33] Raza J, Farooq M, Mebarek-Oudina F and Mahanthesh B 2019 *Multidiscip. Model. Mater.* **15** 913–31
[34] Magyari E and Keller B 1999 *J. Phys.* **32** 577–85
[35] Waqas M, Farooq M, Khan M J, Alsaedi A, Hayat T and Yasmeen T 2016 *Int. J. Heat Mass Transf.* **102** 766–72
[36] Fatunmbi E O, Okoya S S and Makinde O D 2020 *Diffus. Fouundations* **26** 63–77
[37] Dhlamini M, Mondal M, Sibanda P and Motsa S J 2018 *Nanofluids* **7** 917–27
[38] Mandal I C and Mukhopadhyay S 2018 *Mech. Adv. Mater. Struct.* **0** 1–7
[39] Patil P M, Kulkarni M and Hiremath P S 2019 *Arab. J. Sci. Eng.* 1–10
[40] Hayat T, Ullah I, Alsaedi A and Ahamad B 2018 *J Heat Transfer* **140** 1–8
[41] Prasad K V, Vajravelu K and Van-Gorder R A 2011 *Acta. Mech.* **220** 139–54
[42] Mamatha S U, Raju C S K, Mahesha and Makinde O D 2018 *Diffus. Foundations* **16** 177–90
[43] Nayak M K, Shaw S, Makinde O D and Chamkha A J 2019 *J Nanofluids* **8** 51–62
[44] Rahman M M, Aziz A and Al-Lawatia M A 2010 *Int. J. Therm. Sci.* **49** 1–10
[45] Ishak A 2020 *Appl. Math. Comput.* **217** 837–42
[46] Makinde O D 2010 *Int. J. Phys. Sci.* **5** 700–10
[47] Mahanthesh B, Gireesha B J, Gorla R S R and Makinde O D 2018 *Neural. Comput. Appl.* **30** 1557–67
[48] Attili B S and Syam M L 2008 *Chaos Solitons Fractals* **35** 895–903
[49] Mabood F and Das K 2016 *Eur. Phys. J. Plus* **131** 1–13
[50] Xu L and Lee E W M 2013 *Abst. Appl. Anal.* **2013** 1–6
[51] Ali M E 1994 *Wärme- und Stoffübertragung* **29** 227–34
[52] Mabood F and Shateyi S 2013 *Model Simul. Mat. Sci. Eng.* **2019** 1–11